THE JOURNAL OF BIOLOGICAL CHEMISTRY VOL. 286, NO. 47, pp. 40954–40961, November 25, 2011

Structure of Human Na^+/H^+ Exchanger NHE1 Regulatory Region in Complex with Calmodulin and Ca^{2+} [S]◆

Received for publication, July 28, 2011, and in revised form, September 6, 2011 Published, JBC Papers in Press, September 19, 2011, DOI 10.1074/jbc.M111.286906

Stefan Köster[‡], Tea Pavkov-Keller[‡§], Werner Kühlbrandt[‡], and Özkan Yildiz[‡1]

From the [‡]Department of Structural Biology, Max Planck Institute of Biophysics, Max-von-Laue Str. 3, 60438 Frankfurt am Main, Germany and the [§]Department of Structural Biology, Institute of Molecular Biosciences, University of Graz, Humboldtstrasse 50/3, 8010 Graz, Austria

Background: The human Na^+/H^+ exchanger NHE1 is activated through binding of calmodulin.
Results: We determined the x-ray structure of the NHE1 regulatory region in complex with calmodulin and calcium.
Conclusion: The complex structure serves as a basis for a transport regulatory model.
Significance: The complex structure improves our understanding of the medically important NHE1.

The ubiquitous mammalian Na^+/H^+ exchanger NHE1 has critical functions in regulating intracellular pH, salt concentration, and cellular volume. The regulatory C-terminal domain of NHE1 is linked to the ion-translocating N-terminal membrane domain and acts as a scaffold for signaling complexes. A major interaction partner is calmodulin (CaM), which binds to two neighboring regions of NHE1 in a strongly Ca^{2+}-dependent manner. Upon CaM binding, NHE1 is activated by a shift in sensitivity toward alkaline intracellular pH. Here we report the 2.23 Å crystal structure of the NHE1 CaM binding region ($NHE1_{CaMBR}$) in complex with CaM and Ca^{2+}. The C- and N-lobes of CaM bind the first and second helix of $NHE1_{CaMBR}$, respectively. Both the NHE1 helices and the Ca^{2+}-bound CaM are elongated, as confirmed by small angle x-ray scattering analysis. Our x-ray structure sheds new light on the molecular mechanisms of the phosphorylation-dependent regulation of NHE1 and enables us to propose a model of how Ca^{2+} regulates NHE1 activity.

The sodium/proton exchangers (NHEs)[2] of the solute carrier 9 (SLC9) family are secondary transporters found in a wide variety of tissues of all animal species and have homologues in all kingdoms of life (1, 2). Plasma membrane NHEs use the chemical energy of the Na^+ gradient across the plasma membrane for electroneutral counter-transport of H^+ (3, 4). So far, 10 different mammalian NHE isoforms of 25–70% amino acid identity have been identified and characterized (2, 5). The type-1 Na^+/H^+ exchanger NHE1 (6) is ubiquitous in the plasma membrane of virtually all mammalian cells, where it regulates intracellular pH, salt concentration, and cell volume (4, 7). NHE1 is therefore critical for the control and maintenance of some of the most fundamental processes in cellular physiology, including cell growth and differentiation (7). For human health and disease, NHE1 plays crucial roles in heart hypertrophy (8, 9), cardiac ischemia (10), and hypertension (11).

NHE1 has two functional modules: an N-terminal ion translocation domain of ~500 amino acids with 12 or 14 predicted transmembrane helices and a regulatory C-terminal, cytoplasmic domain of ~300 amino acids (12, 13). The C-terminal domain exerts its regulatory function by phosphorylation and by association with a number of signaling molecules. In particular, phosphatidylinositol 4,5-bisphosphate binds to the juxtamembrane region, actin-binding proteins of the ezrin, radixin, moesin (ERM) family connect NHE1 to the cytoskeleton, and various serine kinases such as the ERK-regulated kinase p90RSK, the Ste20-like Nck-interacting kinase (NIK), and the Rho-associated kinase p160ROCK phosphorylate NHE1 near the C terminus (reviewed in Ref. 14). The second messenger Ca^{2+} is involved in NHE1 regulation via four Ca^{2+}-binding EF-hand proteins. Although calcineurin B homologous proteins 1 and 2 (CHP1 and CHP2) (15, 16) and tescalcin (CHP3) (17) bind to the juxtamembrane region of NHE1, calmodulin (CaM) binds to two neighboring sites in the C-terminal regulatory domain. CaM binds with high affinity (K_d ~20 nM) to a binding region defined by residues 637–657 and with intermediate affinity (K_d ~350 nM) to a second region of residues 657–700 (18). An autoinhibitory region in the C-terminal domain, which suppresses NHE1 activity by reducing the affinity for intracellular H^+ (19), overlaps with the first CaM binding region. Upon the binding of Ca^{2+}/CaM, the activation profile of NHE1 shifts toward alkaline intracellular pH (18, 20). In the sarcolemma, this activation is inhibited by preventing CaM binding through phosphorylation of a serine residue (Ser-648) by protein kinase B/Akt (PKB/Akt) during intracellular acidosis (21).

It is thought that a region upstream of the NHE1 regulatory domain (residues 516–590) can interact with the CaM binding region (22), whereas mutation of an acidic cluster in a downstream region (residues 753–759) decreases CaM binding and results in reduced Na^+/H^+ exchange activity (23). Although biochemical data describing Ca^{2+}/CaM binding to NHE1 have been reported, the binding mechanism by which Ca^{2+}/CaM

◆ This article was selected as a Paper of the Week.
The atomic coordinates and structure factors (code 2YGG) have been deposited in the Protein Data Bank, Research Collaboratory for Structural Bioinformatics, Rutgers University, New Brunswick, NJ (http://www.rcsb.org/).
[S] The on-line version of this article (available at http://www.jbc.org) contains supplemental Figs. S1 and S2.
[1] To whom correspondence should be addressed. Tel.: 49-69-6303-3051; Fax: 49-69-6303-3002; E-mail: Oezkan.Yildiz@biophys.mpg.de.
[2] The abbreviations used are: NHE, sodium/proton exchanger; CaM, calmodulin; CaMBR, CaM binding region; SAXS, small angle x-ray scattering.

activates NHE1 has remained elusive. In the classical binding mode, the two lobes of CaM wrap around a target sequence, thus exposing hydrophobic grooves that interact with hydrophobic anchor residues of the target molecule (24). Often the target sequence of CaM forms an amphipathic helix (25, 26). However, CaM can adopt a wide spectrum of conformations upon binding to a target sequence (24), making it difficult to predict how CaM binds to NHE1.

NHE1 appears to be allosterically regulated by H^+ (19, 20), but the regulatory mechanism has so far remained unclear. According to an early hypothesis, NHE1 has a second H^+ binding site, which functions as a sensor and is distinct from the transport site (27). Although this is commonly accepted, more recent studies suggest that intracellular acidification increases the H^+ affinity of NHE1 without requirement for a H^+ sensor (28). Notwithstanding its great biological and medical importance, information on the structure and molecular mechanism of NHE1 is largely lacking. So far, only the structure of the juxtamembrane region of the regulatory domain (amino acids 503–545) in complex with CHP1 or CHP2 has been determined by NMR (29) or x-ray crystallography (30).

Here we present the crystal structure of human $NHE1_{CaMBR}$ in complex with CaM and Ca^{2+}. We show how CaM interacts with both CaM binding sites in NHE1 and provide insights into how posttranslational modification by phosphorylation affects CaM binding and results in the stimulation or inhibition of NHE1 activity. Furthermore, the structure reveals a new CaM binding mode, and we propose an extended model of NHE1 modulation by its C-terminal regulatory domain.

EXPERIMENTAL PROCEDURES

Protein Expression and Purification—The gene segment encoding residues 622–690 of human NHE1 (calmodulin binding region, $NHE1_{CaMBR}$) was codon-optimized for overexpression in *Escherichia coli* (GenScript, Piscataway, NJ) and inserted into the vector pGEX6P1 (GE Healthcare) to produce $NHE1_{CaMBR}$ with an N-terminally fused GST tag. The gene for production of tag-free calmodulin was inserted via NcoI and XhoI into the expression vector pET28a.

E. coli C41 (DE3) cells (Avidis, Saint-Beauzire, France) were sequentially transformed with the two recombinant plasmids. An overnight pre-culture was transferred to terrific broth medium containing 100 μg/ml ampicillin and 50 μg/ml kanamycin. Upon reaching an A_{600} 1.5 at 37 °C, the protein expression was induced with 1 mM isopropyl β-D-1-thiogalactopyranoside, and the temperature was decreased to 28 °C. After expression for 4 h, the cells were pelleted, resuspended in lysis buffer (50 mM Tris-HCl, pH 7.7, 100 mM NaCl, 5 mM $CaCl_2$), and disrupted using a Microfluidizer (M-110L, Microfluidics Corp., Newton, MA). After 1 h of centrifugation at 12,000 × *g*, the cell-free supernatant was applied to a glutathione-Sepharose 4B column (GE Healthcare). The GST-$NHE1_{CaMBR}$/Ca^{2+}/CaM complex was eluted with lysis buffer containing 20 mM glutathione, incubated overnight at 4 °C with PreScission protease (GE Healthcare) for cleavage of the fusion protein into $NHE1_{CaMBR}$ and GST, and concentrated using a Vivaspin 10,000 molecular weight cut-off filter (Sartorius). The concentrated protein was then gel-filtered on a HiLoad 16/60 Superdex 200 (GE Healthcare) size exclusion chromatography column pre-equilibrated with S200 buffer (20 mM Tris-HCl, pH 7.7, 20 mM NaCl, 2 mM $CaCl_2$). Fractions containing the $NHE1_{CaMBR}$/Ca^{2+}/CaM complex were pooled and loaded twice onto the glutathione-Sepharose 4B column to remove the GST. The flow-through containing the complex was collected, concentrated (Vivaspin 10,000 molecular weight cut-off filter, Sartorius), flash-frozen in liquid nitrogen, and stored at −80 °C. The CaM binding regions of residues 604–657 or 652–693 were produced in the same way. For analytical size exclusion chromatography, CaM was expressed and purified using the plasmid provided by Dr. Wei-Jen Tang's laboratory according to an established protocol (31).

Analytical Size Exclusion Chromatography—The apparent size of Ca^{2+}/CaM in the presence and absence of $NHE1_{CaMBR}$ was analyzed by size exclusion chromatography (Superdex 75 PC3.2/30) in S200 buffer. Protein elution was monitored at 280 nm, and protein-containing fractions were analyzed by SDS-PAGE.

Crystallization and Data Collection—For three-dimensional crystallization, the $NHE1_{CaMBR}$/Ca^{2+}/CaM complex was concentrated to 10 mg/ml. Initial crystallization conditions were found in 96-well hanging drop plates using commercial crystallization screens (Hampton Research) and a Mosquito pipetting robot (Molecular Dimensions). Equal volumes (400 nl) of protein and reservoir were mixed and incubated at 18 and 4 °C against 100 μl of reservoir solution. Several crystallization conditions yielded small needle-like crystals, which were optimized in 24-well plates. The best crystals grew within 2 weeks at 4 °C in hanging drops by mixing 1 μl of protein (10 mg/ml) and 2 μl of reservoir solution containing 100 mM Tris, pH 7.0, 12% (w/v) PEG 3350, 20% (v/v) 2-Methyl-2,4-pentanediol, and 80 mM ammonia acetate. For data collection, crystals were transferred to the reservoir solution and flash-frozen in liquid nitrogen. Diffraction data from a long, thin plate were collected at the beamline PXII at the Swiss Light Source (SLS) and processed with the XDS software package (32).

Structure Determination and Refinement—The structure was solved by molecular replacement with a polyalanine model of two copies of the fragment 9–73 of calmodulin in complex with trifluoperazine (Protein Data Bank (PDB) ID 1A29 (33)) with the program PHASER (34) from the CCP4 package (35). The initial electron density map obtained from PHASER covering only the search model was extended automatically by cycles of density modification, automatic model building using RESOLVE (36), and refinement by REFMAC5 (37). This procedure built 60% of the $NHE1_{CaMBR}$ sequence as an alanine model and docked 80% of the density into the resulting map. The model was subjected to iterative rounds of rebuilding into $2F_o - F_c$ and $F_o - F_c$ electron density maps and refined using the phenix.refine subroutine from the PHENIX program suite (38). Data collection, refinement, and model statistics are summarized in Table 1. Figures were generated by PovScript+ (39) and POV-Ray. Superpositions were carried out with the SSM (40) superposition routine from COOT.

Small-angle X-ray Scattering—Small-angle x-ray scattering of the $NHE1_{CaMBR}$/Ca^{2+}/CaM complex was measured on the European Molecular Biology Laboratory (EMBL) Hamburg/

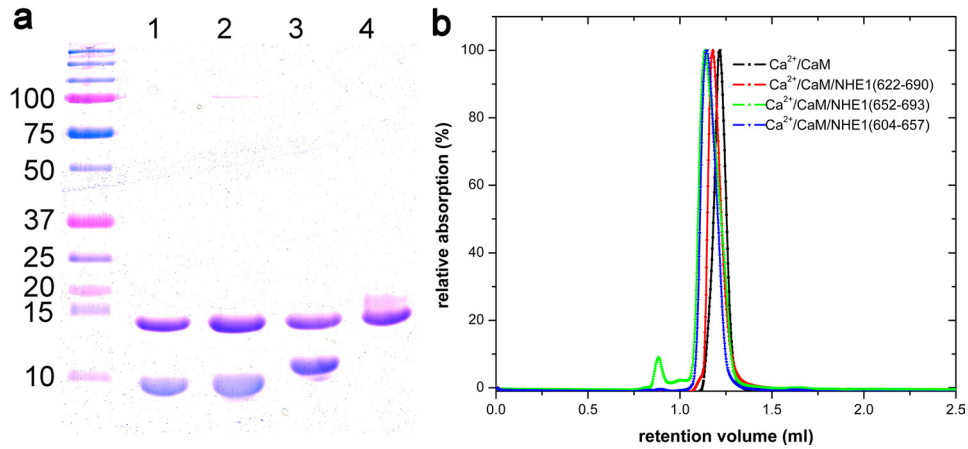

FIGURE 1. **Analysis of the complexes of CaM with different NHE1-fragments.** *a*, SDS-PAGE shows the purity of CaM co-eluted with $NHE1_{604-657}$ (*lane 1*), $NHE1_{652-693}$ (*lane 2*), and $NHE1_{622-690}$ (*lane 3*). *Lane 4* shows the non-complexed apoCaM. *b*, size exclusion chromatography of these complexes shows a monodisperse peak at nearly the same retention volume.

Deutsches Elektronen Synchrotron (DESY) beamline X33 with a MAR345 image plate detector at a sample-detector distance of 2.7 m and a wavelength of $\lambda = 0.15$ nm. The exposure time per measurement was 120 s. Solutions with protein concentrations of 2.9, 6.4, or 10.3 mg/ml as determined using the J357 automatic refractometer (Rudolph Research Analytical, Hackettstown, NJ) were measured at 18 °C. Data analysis was performed with PRIMUS (41). Forward scattering *I(0)* and radius of gyration R_g were determined from Guinier analysis (42). Distance distribution function *P(r)* and maximum particle dimensions D_{max} were determined with the program GNOM (43). Molecular masses of solutes were estimated from small angle x-ray scattering (SAXS) data by comparing extrapolated forward scattering with the data of a bovine serum albumin solution (4.2 mg/ml, $M_r = 66{,}000$).

The low-resolution *ab initio* shape of the $NHE1_{CaMBR}/Ca^{2+}$/CaM complex was reconstructed in GASBOR (44). Ten GASBOR runs were performed (supplemental Fig. S1), and models were averaged to determine common structural features by using the programs SUPCOMB (45) and DAMAVER (46). The scattering curve of the $NHE1_{CaMBR}/Ca^{2+}$/CaM x-ray structure was calculated with the program CRYSOL (47).

TABLE 1
Data collection and refinement statistics
AU, asymmetric unit; r.m.s., root mean square.

	$NHE1_{CaMBR}/Ca^{2+}$/CaM
Data collection	
Space group	C121
Cell dimensions (Å)	$a = 201.28$, $b = 38.37$, $c = 34.11$ $\alpha = \gamma = 90.0°$, $\beta = 91.4°$
Matthews coefficient ($Å^3Da^{-1}$)	2.73
Solvent content (%)	55.03
No. of molecules per AU	1
Resolution (Å)	20–2.23 (2.40–2.23)
Wavelength (Å)	$\lambda = 0.978$
X-ray source	PXII (Swiss Light Source)
R_{meas}* (%)	14.8 (69.7)
R_{mrgd-F}* (%)	8.6 (32.2)
I/Iσ	16.52 (5.93)
Completeness (%)	96.0 (83.3)
No. of observed reflections	156,701 (23092)
No. of unique reflections	12,449 (2100)
Refinement	
Resolution (Å)	30–2.23
No. of unique reflections	12,447
No. of reflections in test set	623
R_{work}/R_{free} (%)	17.34/23.17
No. of atoms in AU	1885
No. of water molecules	114
Wilson *B*-factor ($Å^2$)	28.84
r.m.s. deviations	
Bond lengths (Å)	0.010
Bond angles (°)	1.156

* As defined by Diedrichs and Karplus (REF) (55).

RESULTS

$NHE1_{CaMBR}$, CaM, and Ca^{2+} Form Ternary Complexes—Expression and purification of the CaM binding region (CaMBR, residues 622–690) without CaM were not possible due to proteolytic degradation of $NHE1_{CaMBR}$. Co-expression with CaM prevented degradation and enabled high-yield production of a $NHE1_{CaMBR}$/CaM complex. Fragments containing only one CaM binding site (residues 604–657 or 652–693) of $NHE1_{CaMBR}$ in complex with CaM were expressed separately at high yield. The three complexes of CaM with the entire $NHE1_{CaMBR}$ or with each individual binding site were co-purified to homogeneity in the presence of Ca^{2+}. The complexes were monodisperse as shown by SDS-PAGE and analytical size exclusion chromatography (Fig. 1). When Ca^{2+} was removed by EGTA chelation, the $NHE1_{CaMBR}$/CaM complex dissociated and $NHE1_{CaMBR}$ degraded successively, demonstrating the importance of Ca^{2+} for complex formation and stability.

Crystal Structure Determination and Overall Structure of the Complex—The stability of the NHE1 CaM binding sites in complex with CaM and Ca^{2+} prompted us to try crystallization. Crystals were obtained only with the $NHE1_{CaMBR}/CaM/Ca^{2+}$ complex containing both CaM binding sites. The complex produced monoclinic, needle-like plates (cell parameters: $201.28 \times 38.37 \times 34.11$ $Å^3$, $\beta = 91.4°$) with one molecule in the asymmetric unit, which after optimization diffracted to 2.23 Å resolution. The structure was solved by molecular replacement with CaM and was refined to an *R*-factor and R_{free} factor of 17.34 and 23.17%, respectively (Table 1).

The overall structure shows a 1:1 binding stoichiometry of the $NHE1_{CaMBR}$ and CaM. The final model of the complex includes amino acids 622–684 of $NHE1_{CaMBR}$ and 5–148 of CaM. $NHE1_{CaMBR}$ forms two α-helices linked by a short stretch of four amino acids (Fig. 2*a*). CaM is in an elongated conforma-

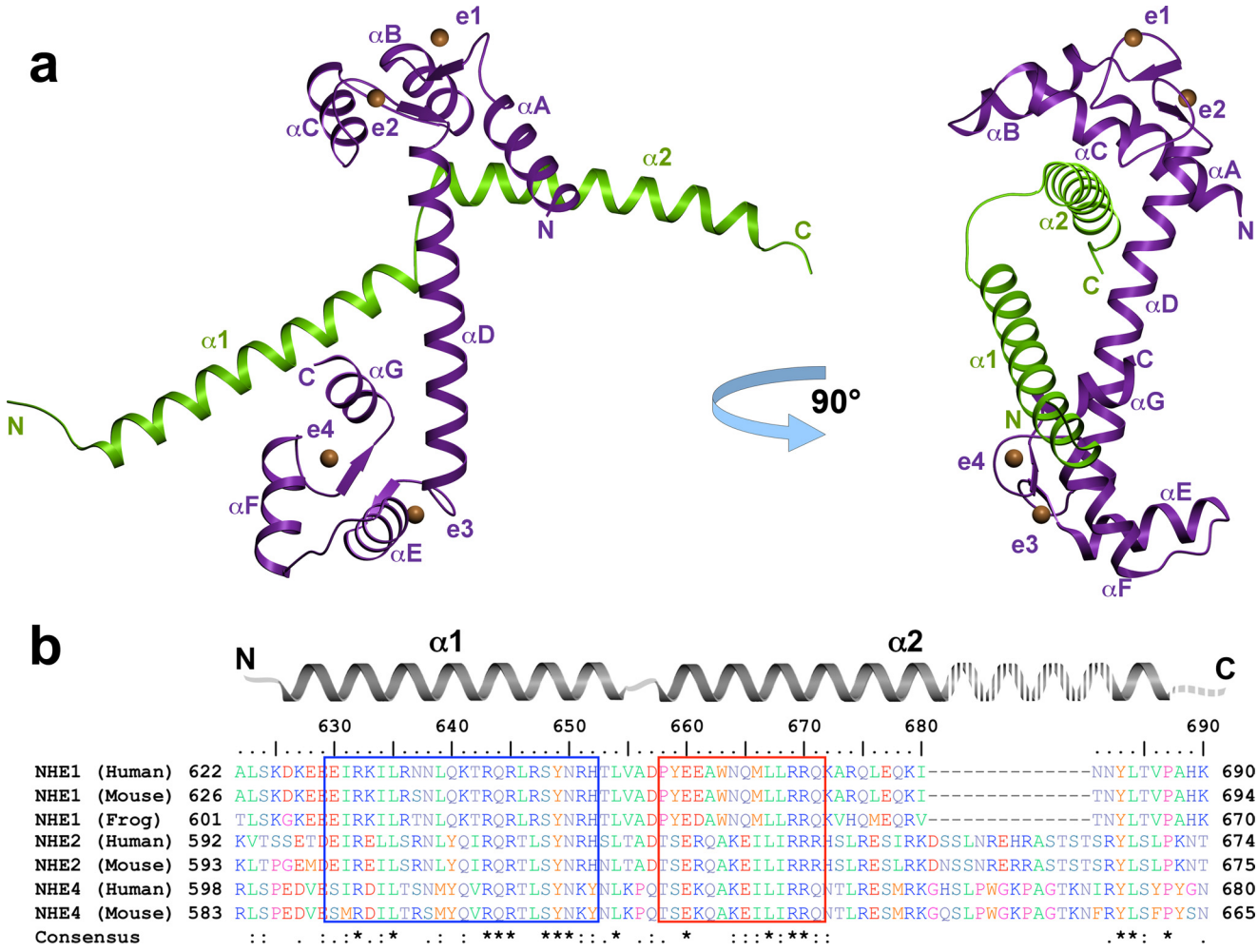

FIGURE 2. **Overall structure of the NHE1$_{CaMBR}$/Ca^{2+}/CaM complex and sequence alignment of selected mammalian NHE calmodulin binding regions.** *a*, NHE1$_{CaMBR}$ (*green*) consists of two α-helices (α1 and α2) connected by a short loop. CaM (*purple*) is present in an elongated form with a central helix (αD) connecting both lobes, which bind to both NHE1$_{CaMBR}$ helices. Each EF-hand of CaM (indicated as *e1*–*e4*) binds one Ca^{2+} ion (*orange spheres*). *b*, in the sequence alignment of the crystallized human NHE1 fragment with the corresponding sequences of human NHE2 and NHE4, mouse NHE1, NHE2, and NHE4, as well as frog NHE1, both CaM-interacting regions are marked by a *blue* and *red box*.

tion, with the N- and C-lobes connected by a long helix (αD). Each of the four EF-hand motifs binds one Ca^{2+} ion. CaM binds to the two helices of the NHE1 CaM binding region in an antiparallel arrangement, whereby helix α1 of NHE1$_{CaMBR}$ interacts with the C-lobe, whereas helix α2 interacts with the N-lobe of CaM. Remarkably, the binding modes of both lobes are different; helix α2 engages with the hydrophobic cleft of the N-lobe, whereas helix α1 binds to the back of the corresponding cleft of the C-lobe. Unusually, both CaM binding sites are thus associated with the same side of the target region.

To compare the CaMBRs of mammalian NHEs, we aligned the sequences of human and mouse NHE1, NHE2, and NHE4 as well as of frog NHE1 (Fig. 2*b*). The first CaM binding site in helix α1 is characterized by a high degree of sequence conservation, whereas the sequence of the second CaM binding site in helix α2 is less conserved, especially in NHE2 and NHE4. Except for residues at the end of helix α2 (residues 682–687 in human NHE1) and in the linker region between helix α1 and α2, sequences outside the CaMBR are not conserved.

Binding Interfaces—Helix α1, the first CaM binding site of NHE1, interacts with the CaM C-lobe through ionic and hydrophilic contacts along an ~20 Å line of basic residues on its surface. Hydrophobic residues are clustered on the opposite side of helix α1 (Fig. 3*a*), making this helix amphiphilic. Polar and basic residues that interact with CaM in our structure are conserved, in particular three arginines (Arg-632, Arg-643, and Arg-651) and two glutamines (Gln-640 and Gln-644), as well as the hydrophobic residues on the opposite helix surface (Fig. 2*b*). By contrast, helix α2 of the second CaM binding site in NHE1 is not amphiphilic. The interface between this helix and CaM differs in character from helix α1 as it consists of hydrophobic, hydrophilic, and ionic residues (Figs. 2*b* and 3b). At the start of helix α2, a prominent tyrosine side chain (Tyr-659) projects into a hydrophobic pocket on the surface of the bound CaM, where it is in van der Waals contact with seven hydrophobic side chains (Phe-19, Ile-27, Met-51, Val-55, Phe-68, Met-71, and Met-72). The specificity of this interaction is ensured by a hydrogen bond of the Tyr hydroxyl group with the backbone carbonyl of Met-51 via a trapped water molecule. Another con-

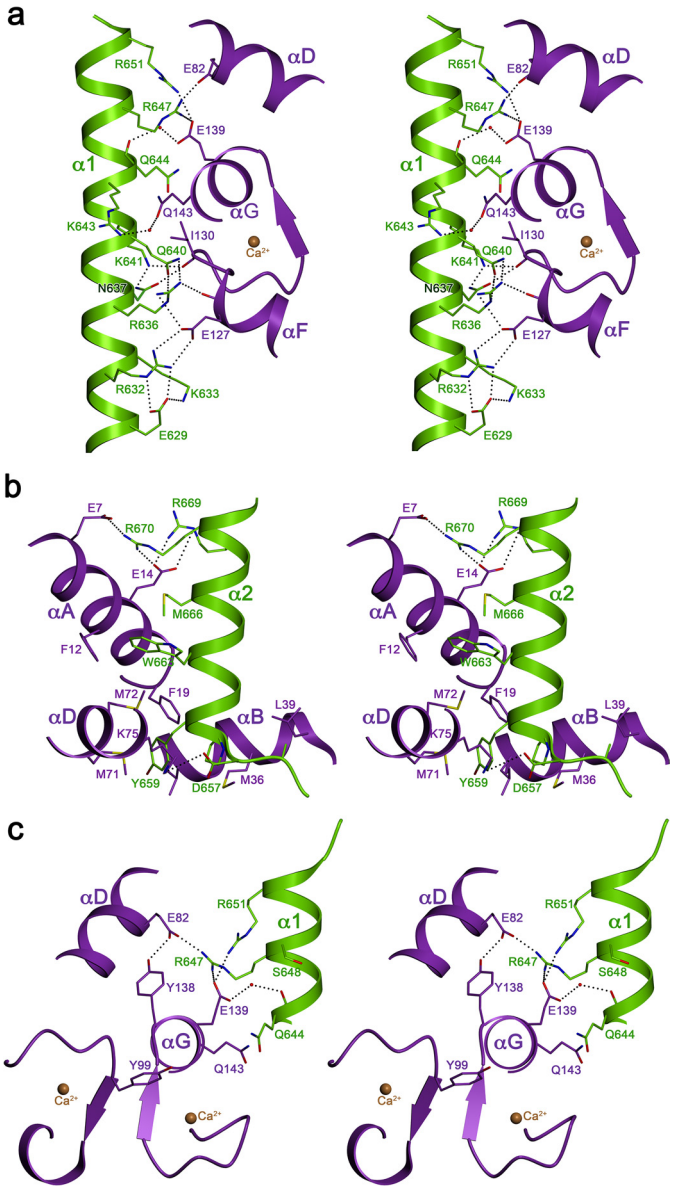

FIGURE 3. **Three-dimensional stereo view of the binding interfaces.** *a*, the first binding interface between the C-terminal lobe of CaM and the first helix of $NHE1_{CaMBR}$ contains mainly charged residues with basic residues of NHE1 and acidic residues of CaM. *b*, the second binding site between the N-terminal lobe of CaM and second helix (α2) of $NHE1_{622-690}$ contains mixed interactions including Trp-663 and Tyr-659 of NHE1 buried into a hydrophobic pocket of CaM and basic NHE1 residues interacting with acidic residues of CaM. *c*, the proposed phosphorylation sites of CaM (Tyr-99 and Tyr-138) and of $NHE1_{CaMBR}$ (Ser-648) are depicted.

FIGURE 4. **Crystallographic interactions between $NHE1_{CaMBR}/Ca^{2+}$/CaM complexes.** A three-dimensional stereo view of the $NHE1_{CaMBR}/Ca^{2+}$/CaM complex with two symmetry-related neighboring complexes (complex 1 and complex 2) is shown. The crystallographic interaction of the complex with complex 1 is mediated by the C-lobe of CaM, which is tightly attached to the N-terminal helix (α1) of $NHE1_{CaMBR}$ (*arrow*). The four CaM EF-hands with bound calcium (*orange spheres*) are indicated as *e1–e4*.

spicuous bulky residue in helix α2 is Trp-663. In the CaM-$NHE1_{CaMBR}$ complex, this tryptophan is surrounded by the hydrophobic side chains Phe-12, Ala-15, Phe-68, Met-72, and Met-76 of CaM, plus Leu-667 and Met-666 of NHE1. In the hydrophobic environment defined by these residues, the indole group of Trp-663 is sandwiched between two methionines from both binding partners ($Met\text{-}666_{NHE1}$ and $Met\text{-}72_{CaM}$). At the end of the second binding site, two basic residues in NHE1 (Arg-669 and Arg-670) and two acidic residues of CaM (Glu-7 and Glu-11) form strong ion pairs. The two arginines are conserved in the NHEs interacting with CaM (Fig. 2*b*), whereas, surprisingly, this is not the case for the prominent hydrophobic residues Tyr-659, Trp-663, and Met-666 that are relevant for complex formation.

SAXS Confirms Elongated Binding Mode—Normally, CaM wraps around target peptides by unwinding of the long helix that connects the N- and C-terminal lobes (24). The elongated conformation of CaM in the $NHE1_{CaMBR}/CaM/Ca^{2+}$ complex is thus unusual. This, and the observation that helix α1 in the crystal structure forms another hydrophobic interaction with the C-lobe of a symmetry-related CaM (Fig. 4), prompted us to ask whether a compact conformation of the complex, with both CaM lobes wrapped around a single binding region, might also be possible, or even preferred, under solution conditions. We therefore investigated the low-resolution solution structure of the complex by SAXS.

X-ray scattering curves obtained with a range of concentrations indicated a molecular mass of 26.5 ± 2 kDa, a radius of gyration of 23.3 ± 0.5 Å, and a longest dimension of 81 ± 3 Å for the $NHE1_{CaMBR}/Ca^{2+}$/CaM complex. These parameters are in excellent agreement with those calculated from the crystal structure as 25.9 kDa, 24.7 Å, and 81 Å, respectively, indicating only minor differences between the x-ray and solution structures of the complex. The scattering curves and the distance

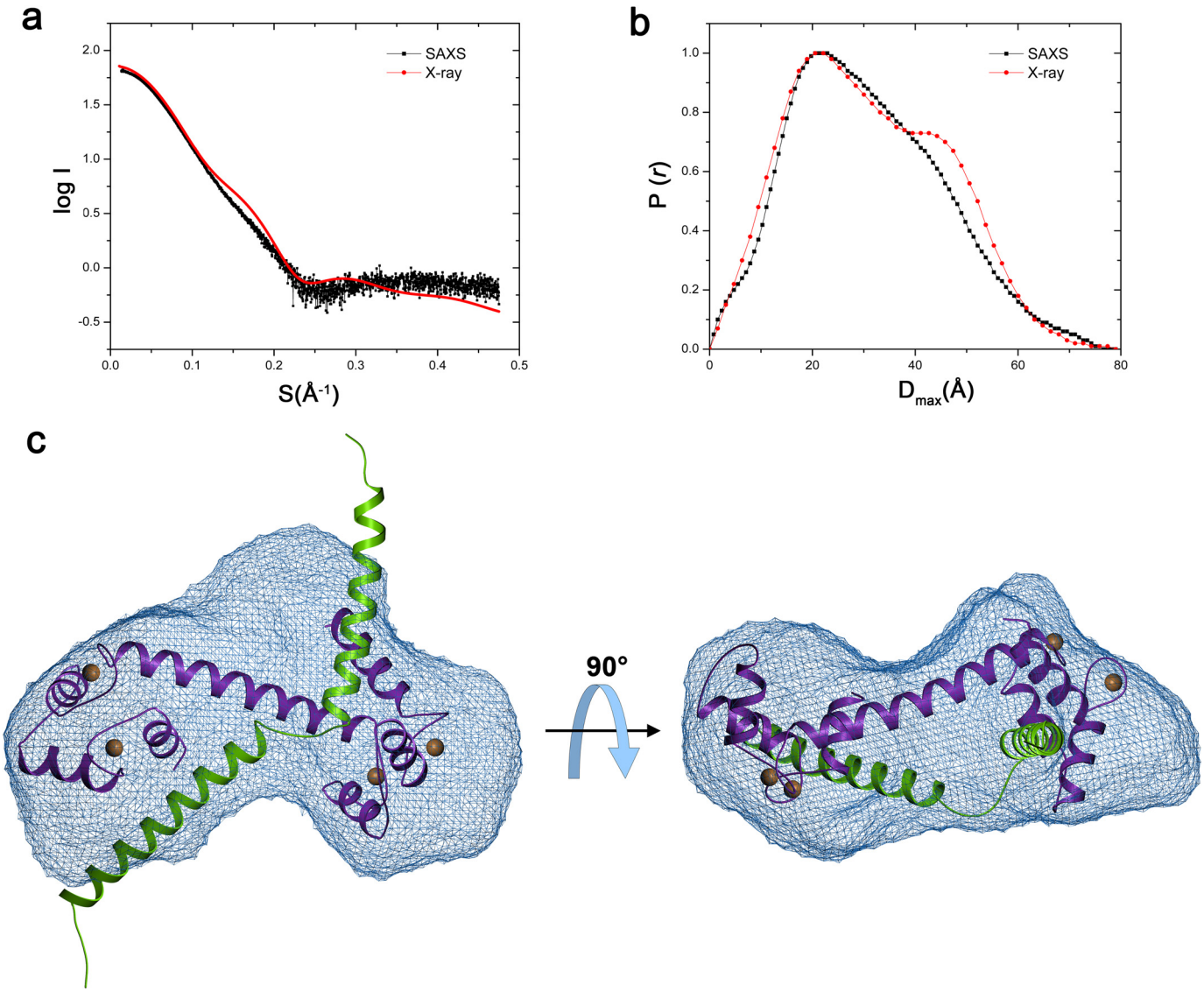

FIGURE 5. **SAXS analysis of the NHE1$_{CaMBR}$/Ca^{2+}/CaM complex structure in solution.** *a* and *b*, experimentally acquired scattering curves (*black*) of the NHE1$_{CaMBR}$/Ca^{2+}/CaM complex in solution are compared with the calculated curves (*red*) using the crystal structure (*a*) and are used for calculation of distance distribution function (*b*). *c*, a low-resolution envelope was reconstructed (*blue mesh*) in which the crystal structure of the NHE1$_{CaMBR}$/Ca^{2+}/CaM complex was fitted.

distribution function *P(R)* calculated from the crystal structure do not fit the experimental data perfectly (Fig. 5, *a* and b), where a shoulder at D_{max} of 40 – 60 Å was more apparent for the complex structure. However, the deviations were small, and the agreement is fully consistent with a 1:1 stoichiometry of CaM and NHE1$_{CaMBR}$ in the complex. Any differences between the measured and calculated scattering curves can be attributed to flexibility of the NHE1$_{CaMBR}$ helix termini as well as the CaM helix connecting the lobes. The SAXS data show that the complex is monomeric in solution.

We calculated an ensemble of 10 low-resolution shapes of the NHE1$_{CaMBR}$/Ca^{2+}/CaM complex from the experimental SAXS data (supplemental Fig. S1). Superposition of these shapes gave a normalized spatial discrepancy of 1.09 ± 0.035, implying only small variations between individual shapes. The most probable *ab initio* model of the complex, obtained by averaging and filtering all calculated models, is shown as a SAXS envelope (Fig. 5*c* and supplemental Fig. S2). The envelope indicates that the complex is more or less heart-shaped. When the crystal structure is docked into the experimental SAXS envelope, it is evident that CaM is bound to NHE1$_{CaMBR}$ in an elongated form also in solution conditions. The CaM molecule fitted into the SAXS envelope, but the terminal ends of the two NHE1 helices of the crystal structure were sticking out. As shown in Fig. 4, the terminal ends of NHE1$_{CaMBR}$ are involved in crystal packing and thus might be flexible in solution. The α-helix conformation of the N- and C-terminal ends of NHE1$_{CaMBR}$ may consequently be due to crystal contacts.

DISCUSSION

Upon Binding to NHE1, CaM Adopts a New, Elongated Binding Mode—The structure and biochemistry of CaM with and without bound ligands have been studied extensively for many years. In the absence of target proteins, CaM has an elongated shape with a central linker connecting its Ca^{2+} binding N- and C-terminal lobes (24). Generally, CaM binds to target proteins

upon activation by Ca^{2+}. This usually goes along with a conformational change that transforms CaM from its elongated default shape into a compact form, in which the two lobes and connecting helix wrap around the target sequence. Several different types of CaM target sequence are known. A target pattern for CaM binding is the well characterized IQ motif with the consensus sequence (FILV)Q*XXX*(RK)G*XXX*(RK)*XX*(FILVWY), found in CaM target sequences such as the voltage-dependent Ca^{2+} channel $Ca_v1.1$ (48) or the neuronal voltage-dependent sodium channel ($Na_v1.2$) (49). Other target sequences are characterized by the number of residues between bulky side chains in hydrophobic cavities of the N- and C-lobes of CaM (24). These include the so-called 1–16 motif, found in the complex of Ca^{2+}/CaM with calmodulin-dependent protein kinase kinase (CaMKK) (50). However, neither of the above mentioned motifs fits the $NHE1_{CaMBR}$. So far, in other complex structures, CaM resembles a compact globular conformation. An exception is the crystal structure of CaM in complex with a calcineurin peptide (51) where CaM is elongated. However, SAXS measurements have shown that in solution, CaM adopts a compact conformation in this complex (51). Therefore, the elongated form in the calcineurin complex is most likely due to crystal contacts.

By contrast, the crystal structure of the $NHE1_{CaMBR}$/CaM complex, in which CaM resembles the unliganded form closely, is in good agreement with its solution structure (Fig. 5). Therefore, the interaction of CaM with NHE1 represents a new mode of CaM binding stably to a target sequence, in an elongated conformation that resembles the unliganded conformation. Although the binding of helix $\alpha2$ to the hydrophobic pocket of CaM N-lobe can be considered as typical for CaM/target interactions, the C-lobe exclusively contributes ionic and hydrophilic interactions with helix $\alpha1$, whereas its hydrophobic pocket points away from the target sequence and forms crystal contacts with symmetry-related molecules.

Implications for NHE1 Regulation by Ca^{2+}/CaM—Elevated Ca^{2+} concentrations cause CaM to bind to $NHE1_{CaMBR}$ and stimulate sodium-proton exchange. NHE1 activity is further regulated by posttranslational modification in the C-terminal region of the exchanger, which includes the CaM binding domain. Phosphorylation of $NHE1_{CaMBR}$ at Ser-648 by PKB/Akt has a significant impact on NHE1 regulation as it inhibits complex formation between NHE1 and CaM and thus prevents activation (21). Our structure shows that Ser-648 is located centrally in the first CaM binding sites of NHE1, and phosphorylation of this residue would disrupt the interface between helix $\alpha1$ and CaM (Fig. 3*c*). The negative charge of phosphorylated Ser-648 would attract arginines Arg-647 and Arg-651 in the NHE1 sequence. This would in turn prevent the formation of strong salt bridges between these residues and Glu-83 and Glu-140 of CaM, which we observe in our complex structure and consequently would weaken the NHE1/CaM interaction. The negative charge on phosphorylated Ser-648 would repel the negatively charged residues of CaM, weakening the binding affinity further.

In addition to phosphorylation of the NHE1 target sequence, phosphorylation of CaM itself could also affect the interaction with NHE1 and consequently its regulation. It has been proposed that NHE1 is activated by phosphorylation of CaM tyrosines by Janus kinase 2 (Jak2) upon hypertonic stress (52). Moreover, stimulation of the bradykinin B2 (53) or 5-hydroxytryptamine 1A receptor (54) results in NHE1 activation. So far, it is not known whether Jak2 can phosphorylate one or both CaM tyrosines (Tyr-99 or Tyr-138). Our structure shows that both are close to the interface between helix $\alpha1$ and CaM (Fig. 3*c*). We assume that only phosphorylation of Tyr-138 would have an effect on NHE1/CaM complex formation as this could establish an additional salt bridge with arginine Arg-651. The longer distance between Tyr-99 and the target sequence makes a direct interaction less likely.

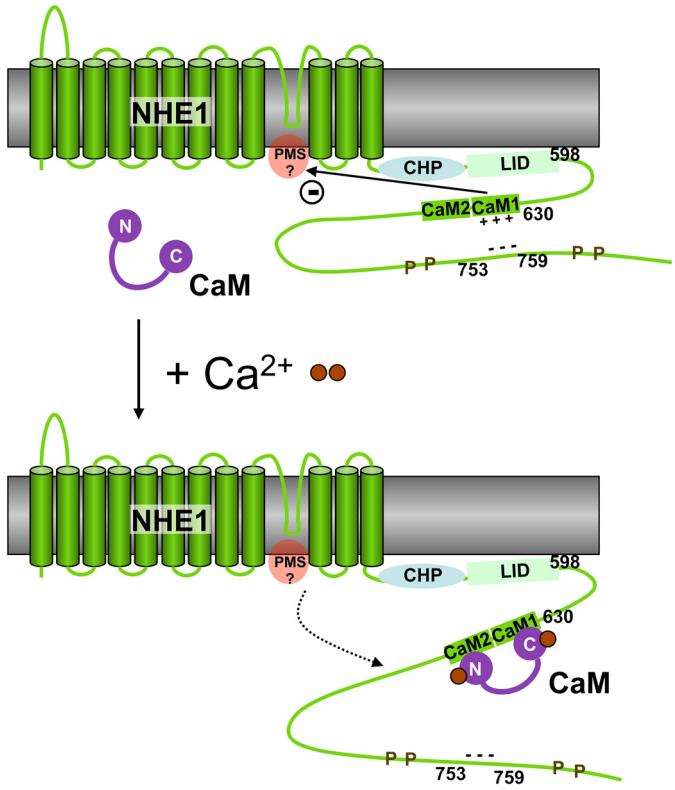

FIGURE 6. **Schematic model of the calcium-dependent regulation of NHE1 by CaM.** The antiporter activity of NHE1 is down-regulated by the autoinhibitory domain within the CaM binding region (*CaM1* and *CaM2*), probably by its interaction with the proton modifier site (*PMS*). The positive charges of CaM1 are neutralized by the binding of an acidic region in the downstream region 753–759, which is flanked by several phosphorylation sites (*P*). Upon the binding of the secondary messenger Ca^{2+} (*brown spheres*), CaM is able to bind to $NHE1_{CaMBR}$, thus replacing the 753–759 region. This would counteract the autoinhibitory domain, resulting in an up-regulation of the NHE1 antiporter activity. *CHP*, calcineurin B homologous protein. *LID*, lipid-interacting domain.

Model for CaM-dependent NHE1 Regulation—Based on the structure of the $NHE1_{CaMBR}$/CaM complex and previous studies by others, we propose a model of NHE1 activation by Ca^{2+}/CaM binding (Fig. 6). In the absence of bound CaM in resting cells with low Ca^{2+} concentration, $NHE1_{CaMBR}$ autoinhibits NHE1, apparently through interaction with the so-called proton modifier site, which is thought to be located in the cytoplasmic region at the C-terminal end of the transmembrane domain (Fig. 6) and to regulate the transport site (20, 27). It is also thought that in this resting state, $NHE1_{CaMBR}$ interacts with an acidic cluster roughly 100 amino acids downstream (23)

and that this interaction stabilizes $NHE1_{CaMBR}$ in a conformation that promotes CaM binding. This is consistent with our observation that all basic amino acids of the CaMBR are located on the same side of the amphiphilic helix α1. CaM binds to $NHE1_{CaMBR}$ at increased Ca^{2+} concentration. The complex structure presented here shows that CaM binds to helix α1 only from this side.

The binding of the autoinhibitory site to the proton modifier site would make access for protons more difficult due to unfavorable electrostatic interactions. CaM binding to one side of helix α1 would weaken the interactions on the opposite side of this helix. The residues on this opposite side of the helix are more highly conserved (Fig. 2), consistent with a possible role in regulation. In our model (Fig. 6), CaM binding would weaken the interaction of the autoinhibitory region with the proton modifier site. Protons would then have unhindered access to this site to up-regulate the transport activity of NHE1.

Our structure adds an important piece to the puzzle of intricate inter- and intramolecular interactions that regulate the activity of this essential exchanger and thus control many basic physiological functions in eukaryotic cells. Further work to confirm our model of NHE1 regulation by CaM is in progress.

Acknowledgments—We thank the staff of the beamline PXII of Swiss Light Source, Villigen, Switzerland and of the European Molecular Biology Laboratory (Hamburg Outstation) for excellent facilities and assistance during data collection. We thank Wei-Jen Tang and Yuequan Shen (University of Chicago) for providing the rat calmodulin construct, Eva Schweikhard for help with crystallization, and Heidi Betz for excellent technical assistance.

REFERENCES

1. Brett, C. L., Donowitz, M., and Rao, R. (2005) *Am. J. Physiol. Cell Physiol.* **288,** C223–C239
2. Orlowski, J., and Grinstein, S. (2004) *Pflugers Arch.* **447,** 549–565
3. Counillon, L., and Pouysségur, J. (2000) *J. Biol. Chem.* **275,** 1–4
4. Pouysségur, J., Franchi, A., L'Allemain, G., and Paris, S. (1985) *FEBS Lett.* **190,** 115–119
5. Lee, S. H., Kim, T., Park, E. S., Yang, S., Jeong, D., Choi, Y., and Rho, J. (2008) *Biochem. Biophys. Res. Commun.* **369,** 320–326
6. Sardet, C., Franchi, A., and Pouysségur, J. (1989) *Cell* **56,** 271–280
7. Grinstein, S., Rotin, D., and Mason, M. J. (1989) *Biochim. Biophys. Acta* **988,** 73–97
8. Chen, L., Gan, X. T., Haist, J. V., Feng, Q., Lu, X., Chakrabarti, S., and Karmazyn, M. (2001) *J. Pharmacol. Exp. Ther.* **298,** 469–476
9. Engelhardt, S., Hein, L., Keller, U., Klämbt, K., and Lohse, M. J. (2002) *Circ. Res.* **90,** 814–819
10. Allen, D. G., and Xiao, X. H. (2003) *Cardiovasc. Res.* **57,** 934–941
11. Phan, V. N., Kusuhara, M., Lucchesi, P. A., and Berk, B. C. (1997) *Hypertension* **29,** 1265–1272
12. Wakabayashi, S., Fafournoux, P., Sardet, C., and Pouysségur, J. (1992) *Proc. Natl. Acad. Sci. U.S.A.* **89,** 2424–2428
13. Goswami, P., Paulino, C., Hizlan, D., Vonck, J., Yildiz, O., and Kühlbrandt, W. (2011) *EMBO J.* **30,** 439–449
14. Baumgartner, M., Patel, H., and Barber, D. L. (2004) *Am. J. Physiol. Cell Physiol.* **287,** C844–C850
15. Lin, X., and Barber, D. L. (1996) *Proc. Natl. Acad. Sci. U.S.A.* **93,** 12631–12636
16. Pang, T., Wakabayashi, S., and Shigekawa, M. (2002) *J. Biol. Chem.* **277,** 43771–43777
17. Zaun, H. C., Shrier, A., and Orlowski, J. (2008) *J. Biol. Chem.* **283,** 12456–12467
18. Bertrand, B., Wakabayashi, S., Ikeda, T., Pouysségur, J., and Shigekawa, M. (1994) *J. Biol. Chem.* **269,** 13703–13709
19. Wakabayashi, S., Ikeda, T., Iwamoto, T., Pouysségur, J., and Shigekawa, M. (1997) *Biochemistry* **36,** 12854–12861
20. Wakabayashi, S., Bertrand, B., Ikeda, T., Pouysségur, J., and Shigekawa, M. (1994) *J. Biol. Chem.* **269,** 13710–13715
21. Snabaitis, A. K., Cuello, F., and Avkiran, M. (2008) *Circ. Res.* **103,** 881–890
22. Ikeda, T., Schmitt, B., Pouysségur, J., Wakabayashi, S., and Shigekawa, M. (1997) *J. Biochem.* **121,** 295–303
23. Li, X., Ding, J., Liu, Y., Brix, B. J., and Fliegel, L. (2004) *Biochemistry* **43,** 16477–16486
24. Vetter, S. W., and Leclerc, E. (2003) *Eur. J. Biochem.* **270,** 404–414
25. O'Neil, K. T., and DeGrado, W. F. (1990) *Trends Biochem. Sci.* **15,** 59–64
26. Sanyal, G., Richard, L. M., Carraway, K. L., 3rd, and Puett, D. (1988) *Biochemistry* **27,** 6229–6236
27. Aronson, P. S., Nee, J., and Suhm, M. A. (1982) *Nature* **299,** 161–163
28. Lacroix, J., Poët, M., Maehrel, C., and Counillon, L. (2004) *EMBO Rep.* **5,** 91–96
29. Mishima, M., Wakabayashi, S., and Kojima, C. (2007) *J. Biol. Chem.* **282,** 2741–2751
30. Ammar, Y. B., Takeda, S., Hisamitsu, T., Mori, H., and Wakabayashi, S. (2006) *EMBO J.* **25,** 2315–2325
31. Drum, C. L., Yan, S. Z., Sarac, R., Mabuchi, Y., Beckingham, K., Bohm, A., Grabarek, Z., and Tang, W. J. (2000) *J. Biol. Chem.* **275,** 36334–36340
32. Kabsch, W. (1993) *J. Appl. Crystallogr.* **26,** 795–800
33. Vertessy, B. G., Harmat, V., Böcskei, Z., Náray-Szabó, G., Orosz, F., and Ovádi, J. (1998) *Biochemistry* **37,** 15300–15310
34. McCoy, A. J. (2007) *Acta Crystallogr. D Biol. Crystallogr.* **63,** 32–41
35. Collaborative Computational Project, Number 4 (1994) *Acta Crystallogr. D Biol. Crystallogr.* **50,** 760–763
36. Terwilliger, T. (2004) *J. Synchrotron Radiat.* **11,** 49–52
37. Murshudov, G. N., Vagin, A. A., and Dodson, E. J. (1997) *Acta Crystallogr. D Biol. Crystallogr.* **53,** 240–255
38. Zwart, P. H., Afonine, P. V., Grosse-Kunstleve, R. W., Hung, L. W., Ioerger, T. R., McCoy, A. J., McKee, E., Moriarty, N. W., Read, R. J., Sacchettini, J. C., Sauter, N. K., Storoni, L. C., Terwilliger, T. C., and Adams, P. D. (2008) *Methods Mol. Biol.* **426,** 419–435
39. Fenn, T. D., Ringe, D., and Petsko, G. A. (2003) *J. Appl. Crystallogr.* **36,** 944–947
40. Krissinel, E., and Henrick, K. (2004) *Acta Crystallogr. D* **60,** 2256–2268
41. Konarev, P. V., Volkov, V. V., Sokolova, A. V., Koch, M. H. J., and Svergun, D. I. (2003) *J. Appl. Crystallogr.* **36,** 1277–1282
42. Guinier, A. (1939) *Ann. Phys.* (*Paris*) **12,** 161–237
43. Svergun, D. I. (1992) *J. Appl. Crystallogr.* **25,** 495–503
44. Svergun, D. I., Petoukhov, M. V., and Koch, M. H. J. (2001) *Biophys. J.* **80,** 2946–2953
45. Kozin, M. B., and Svergun, D. I. (2001) *J. Appl. Crystallogr.* **34,** 33–41
46. Volkov, V. V., and Svergun, D. I. (2003) *J. Appl. Crystallogr.* **36,** 860–864
47. Svergun, D., Barberato, C., and Koch, M. H. (1995) *J. Appl. Crystallogr.* **28,** 768–773
48. Halling, D. B., Georgiou, D. K., Black, D. J., Yang, G., Fallon, J. L., Quiocho, F. A., Pedersen, S. E., and Hamilton, S. L. (2009) *J. Biol. Chem.* **284,** 20041–20051
49. Feldkamp, M. D., Yu, L., and Shea, M. A. (2011) *Structure* **19,** 733–747
50. Osawa, M., Tokumitsu, H., Swindells, M. B., Kurihara, H., Orita, M., Shibanuma, T., Furuya, T., and Ikura, M. (1999) *Nat. Struct. Biol.* **6,** 819–824
51. Majava, V., and Kursula, P. (2009) *PLoS One* **4,** e5402
52. Garnovskaya, M. N., Mukhin, Y. V., Vlasova, T. M., and Raymond, J. R. (2003) *J. Biol. Chem.* **278,** 16908–16915
53. Lefler, D., Mukhin, Y. V., Pettus, T., Leeb-Lundberg, L. M., Garnovskaya, M. N., and Raymond, J. R. (2003) *Assay Drug Dev. Technol.* **1,** 281–289
54. Turner, J. H., Garnovskaya, M. N., Coaxum, S. D., Vlasova, T. M., Yakutovich, M., Lefler, D. M., and Raymond, J. R. (2007) *J. Pharmacol. Exp. Ther.* **320,** 314–322
55. Diedrichs, K., and Karplus, P. A. (1997) *Nat. Struct. Biol.* **4,** 269–275